RESEARCH ARTICLE

National Science Open
3: 20230065, 2024
https://doi.org/10.1360/nso/20230065

Engineering

Special Topic: Energy Systems of Low Carbon Buildings

Radiative cooling for long-term building energy efficiency: An experimental comparison of seven coatings

Yue He[1,2], Biao Lu[1,2], Jinzhong Fang[1,2], Yue Lei[1,2], Shan Gao[1,2] & Chi Feng[1,2*]

[1]*School of Architecture and Urban Planning, Chongqing University, Chongqing 400045, China;*
[2]*Key Laboratory of New Technology for Construction of Cities in Mountain Area, Ministry of Education, Chongqing University, Chongqing 400045, China*

*Corresponding author (email: fengchi860602@outlook.com)

Received 23 October 2023; Revised 21 February 2024; Accepted 8 March 2024; Published online 12 March 2024

Abstract: Radiative cooling coatings are widely used owing to their excellent cooling performance and energy efficiency. However, there is a lack of comprehensive research on their weather resistance, long-term performance and effects on building load. To fill this research gap, seven coatings were selected for experimental observation and simulation research. The results revealed noticeable differences among different coatings regarding anti-aging properties, cooling performance and building load reduction. Some coatings exhibited yellowing, cracking and peeling after weathering tests, accompanied by a decline in their radiative properties. Long-term tests showed that the cooling performance of all coatings gradually decreased due to natural aging, and the rate of decline was proportional to the weathering of the coatings. Building load simulations revealed the potential effect of coating selection on cooling and heating loads, thereby suggesting that different coatings should be selected based on actual usage scenarios in different climatic zones.

Keywords: radiative cooling coating, weather resistance, long-term cooling performance, building load

INTRODUCTION

Rapid industrialization and population growth have contributed to environmental degradation globally, accompanied by increasingly frequent extreme weather events. The unbearable temperature in summer boosts the use of air conditioners, with a significant increase in electricity consumption, exerting a massive influence on the global energy system. Currently, building energy consumption accounts for approximately 40% of global total energy consumption (the largest proportion) [1,2], while the cooling load accounts for 20% of the total electricity consumption of buildings [3]. Reducing the cooling load of buildings is therefore an energy efficiency priority. In response to this challenge, researchers have proposed “cool” roofing technology that utilizes reflective coatings on building surfaces [4]. This coating reduces the heat transferred into the room and therefore the cooling load through high shortwave reflectivity (in the wavelength band of 0.3–2.5 μm) over the visible and near-infrared spectrum [5]. Although studies have shown that reflective coatings can effectively reduce building surface temperature, heat accumulation and cooling energy consumption [6–9], there is still room for improvement.

© Science Press and EDP Sciences 2024. Published by Science Press and EDP Sciences. This is an Open Access article distributed under the terms of the Creative Commons Attribution License (https://creativecommons.org/licenses/by/4.0), which permits unrestricted use, distribution, and reproduction in any medium, provided the original work is properly cited.

Recently, extensive research has been conducted on "upgraded" reflective coatings with better performance. By combining high shortwave reflectivity and longwave emissivity, passive radiative cooling can provide subambient cooling (i.e., a surface temperature lower than the ambient air temperature) by reflecting the vast majority of solar radiation and strongly emitting heat from the surface into the cold universe in the form of longwave radiation (mostly in the mid-infrared band of 2.5–25 μm) through the atmospheric transmittance window (8–13 μm) [10–12]. This cooling also occurs through a net radiative heat transfer from the object surface to the atmosphere based on the significant temperature difference. Because of these features, radiative cooling acts as an energy-efficient, noiseless and environmentally friendly cooling technology [13]. Indeed, research has confirmed the practical applications of this technology in architecture [14–16], textiles [17–19], electronic equipment [20,21] and communication base stations [22,23]. Utilizing radiative cooling coatings in buildings can significantly decrease the surface and indoor temperature during hot weather, thereby reducing the energy consumption and carbon emissions caused by air conditioners [16,24–27]. For example, Liu *et al*. [28] sprayed the superhydrophobic self-cleaning radiative cooling coating on the concrete-based basement roof, and achieved a cooling of 6.2°C in the basement room. Moreover, Chen *et al*. [29] calculated that when radiative cooling coatings were applied to residential concrete roofs, industrial galvanized steel roofs and commercial multistory building roofs, the monthly cumulative building cooling loads were decreased by 18.5–22.3, 33.7–40.5 and 2.9–3.5 kWh/m^2, respectively, compared with the control building. From the aforementioned studies it can be concluded that radiative cooling coatings offer considerable potential for improving the thermal comfort of buildings and reducing cooling energy consumption.

As the radiative cooling technology develops, the concepts and properties of photonic structures [30,31], nanoparticle-embedded polymer structures [14,32], multilayered or grating metamaterials [33,34] and silvered polymer thin coatings [35,36] have been studied in depth and experimentally verified. Each technology has demonstrated unique radiative properties and extraordinary cooling performance. For example, Fan *et al*. [37] prepared a porous radiative cooling coating based on silica aerogel and titanium dioxide with a shortwave reflectivity of 0.92 and a longwave emissivity of up to 0.97, which resulted in a subambient cooling of 7.8°C at midday under solar radiation of 640 W/m^2. The polyvinylidene fluoride coating prepared by Luo *et al*. [38] exhibited a 0.95 shortwave reflectivity and a 0.93 longwave emissivity. The average temperature drop of the coating in direct sunlight was 7.4°C compared with the ambient air temperature. To sum up, different radiative cooling coatings exhibited variations in their shortwave reflectivity and longwave emissivity, which directly affected their cooling performance and, subsequently, the reduction in cooling load.

Regardless of the effectiveness of radiative properties, successfully reflecting the majority of sunlight is a prerequisite for ensuring daytime radiative cooling. Therefore, the reflectivity of radiative cooling materials must be as high and persistent as possible. Similarly, the longwave emissivity should be maintained close to 1 to dissipate heat as much as possible. However, both high shortwave reflectivity and longwave emissivity can be readily inhibited by material aging [39]. The aging process involves two primary aspects. First, the temperature fluctuations are caused by day-night cycles and seasonal changes. Second, ultraviolet (UV) light from natural sunlight, intense precipitation, as well as the deposition of microbial organisms, dust and harmful organic substances all cause surface contamination and the discoloration of many polymers [39]. Typically, radiative cooling materials should be exposed to a natural state for an extended period, preferably

years [40]. However, owing to time and site constraints, most existing studies have only reported the initial radiative properties and cooling performance of coatings, with minimal research accounting for prolonged aging [41]. In the few studies available, He *et al*. [42] only studied the high-temperature resistance, UV-aging resistance and stain resistance of the radiative cooling coating in the laboratory to predict the long-term cooling performance of the coatings. The result was one-sided as they lacked extended field measurements. Similarly, Chen *et al*. [43] only recorded the cooling performance of the superhydrophobic coating before and after contamination by muddy water, suggesting the coating's long-term cooling performance. The test method was one-sided as the experimental design did not account for the long-term effects of solar radiation and other environmental parameters. Additionally, Bijarniya *et al*. [44] demonstrated the cooling performance of a three-layered radiative coating by exposing it outdoors for one month. However, the lack of supplementary information, such as meteorological parameters, made these results inconclusive. In summary, the existing studies do not convincingly clarify the long-term effectiveness of radiative cooling coatings. Consequently, the application potential of radiative cooling coatings after aging remains unclear.

To clarify these issues, we conducted experimental, simulated and theoretical analyses on the weather resistance, long-term cooling performance and reduction in building loads of seven coatings. In the following section, the materials and methods used are introduced. Subsequently, the experimental and simulation results are presented and analyzed. Finally, the conclusions are drawn.

MATERIALS AND METHODS

In this section, the samples of seven target coatings used for the experiments were first prepared. Next, the radiative properties of these coatings were tested in the laboratory after undergoing temperature cycles and UV-aging. Subsequently, a field experiment was conducted to investigate the natural aging resistance of the coatings and their long-term cooling abilities. Finally, the building loads with different coatings applied to the roofs of office buildings in typical cities in China were simulated using WUFI-Plus.

Materials

Seven water-based paste coatings were collected from the market. These targets were selected due to their differences in chemical components, microscopic structures, market prices and, most importantly, radiative properties. To avoid potential commercial issues, we did not disclose their brands or product names. For differentiation, we labeled them as A–G, with G representing a common white coating as a reference. Approximately 400 fiberless cement slabs with the dimensions of 10 cm × 10 cm × 0.45 cm were evenly divided into seven groups. The top surface of each group was separately sprayed with coatings A–G according to the specific usage instructions of each product. Among them, coating A is a multi-layer nanoparticle-embedded polymer material; coatings B and C are photonic materials; coating D is an ordinary-scale polymer-based material; coatings E, F and G (Reference) are single-layer nanoparticle-embedded polymer materials.

To understand the structure and properties of the seven coatings, the scanning electron microscope (SEM) was used to characterize the surface and cross-section microstructures of the coatings, and the results are

shown in Supplementary information Figures S1 and S2. The surfaces of coatings A–F were generally smooth, while the surface of coating G (Reference) was very rough with numerous fine particles. For the cross-section structures (Figure S2), it can be observed that coatings A–F had a few scattered pores internally, whereas coating G (Reference) exhibited a loose and porous structure. The thicknesses of coatings A–G were 428, 472, 392, 213, 268, 274 and 354 μm, based on the cross-section morphological tests on respective samples. According to Figure S3, the water contact angle of the coatings A–G were 126.1°, 80.3°, 80.5°, 94.8°, 47.0°, 94.3° and 84.3°, respectively, where coating A showed strong hydrophobility. Additionally, the adhesion of the coatings was tested by the cross-cut test (rating assessment refers to the execution of Table S1 in the Supplementary information), and the results are shown in Figure S4 and Table S2. Coating A exhibited the strongest adhesion with a rating 0, followed by coating G (Reference) with a rating 2, then the coating F with a rating 3; the last was coatings B, C, D and E, all of which were rated 4.

Laboratory tests

The spectral reflectivity of the coatings in 300–2500 nm solar spectrum was measured using a UV-visible-near infrared (UV-VIS-NIR) spectrophotometer (HITACHI, UH4150) (Figure 1a). The overall shortwave reflectivity was calculated according to the ASTM G173–03 standard [45] with appropriate modifications (Eq. (1)):

$$\rho = \frac{\sum_{\lambda=300\ \mathrm{nm}}^{2500\ \mathrm{nm}} \rho(\lambda) I(\lambda) \Delta\lambda}{\sum_{\lambda=300\ \mathrm{nm}}^{2500\ \mathrm{nm}} I(\lambda) \Delta\lambda}, \tag{1}$$

where ρ is the shortwave reflectivity of the coating; λ is the wavelength, nm; $\rho(\lambda)$ is the spectral reflectivity of the coating; $I(\lambda)$ is the AM1.5 spectral solar radiation, W/(m^2 nm); $\Delta\lambda$ is the scanning interval, 5 nm in our study.

The hemispherical emissivity of the coatings was directly measured using a hemispherical emittance meter (D&S, AE1/RD1) (Figure 1b). The value recorded by the hemispherical emittance meter represented the average longwave emissivity of the coating in the wavelength band of 3–30 μm. At least three samples of each coating were tested, and the average value was calculated.

To study the weather resistance of the coatings, temperature cyclic and UV-aging tests were performed. The temperature cyclic test was performed according to the JG/T 25–2017 standard [46]. Briefly, the sides and back of the sample were sealed with paraffin wax and immersed in a distilled water bath at 23°C for 18 h. Subsequently, the samples were transferred to a climate chamber (YONGJUN, YJ-STH-4P) (Figure 1c), which was alternately operated for 3 h at 50°C and another 3 h at −20°C for a total of 40 cycles. The coatings' radiative properties were tested and the surface appearance was photographed after 0, 10, 20, 30 and 40 cycles. The UV-aging test was conducted in a UV-aging chamber (AISR&IN, KLD QUV340) (Figure 1d) according to GB/T 1865–2009 [47]. The samples were subjected to 300 UV exposure cycles. Each cycle comprised 1.7 h of UV exposure with a strength of 0.51 W/m^2 at 340 nm and 63 ± 2°C, followed by 0.3 h of water spraying. The test was suspended, the coatings' surface appearance was photographed and the radiative properties were tested at 0, 100, 200, 300, 400 and 600 h, approximately corresponding to Chongqing outdoor aging for 0, 1, 2, 3, 4 and 6 months, respectively.

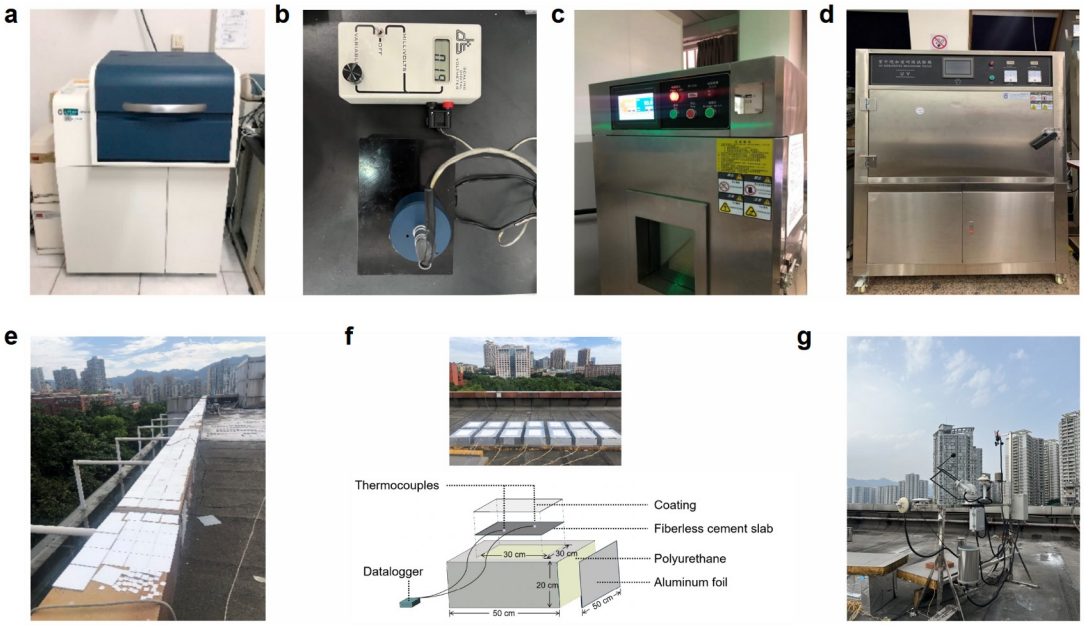


Figure 1 Equipment and setups for laboratory and field tests. (a) HITACHI UH4150 UV-VIS-NIR spectrophotometer; (b) D&S AEIRDI hemispherical emittance meter; (c) YONGJUN YJ-STH-4P climate chamber; (d) AISR&IN KLD QUV340 UV-aging chamber; (e) natural aging test samples; (f) photo (top) and schematic (bottom) of the long-term cooling performance test; (g) meteorological station.

Field measurements

Field measurements were conducted to investigate the effects of natural aging on the surface appearance, radiative properties and long-term cooling performance of the coatings. For the surface appearance and radiative properties (Figure 1e), the samples (with the dimensions of 10 cm × 10 cm × 0.45 cm) were placed on the rooftop of a university building in Chongqing (106.55°E, 29.57°N), China. The test period began on 25 June 2023, and ended on 19 August 2023. For the first six weeks, the coatings' radiative properties were tested and the surface appearance was photographed each week. After that, the radiative properties and surface appearance were recorded biweekly. To maintain the actual condition of the coatings, no additional treatment was applied except for drying the surface moisture before testing the radiative properties.

For the long-term cooling performance (Figure 1f), seven identical scaled-down roof models were constructed and placed side-by-side on an uncovered roof (note: the seven roof models in the front row of the photo had steel plates as bases and were not analyzed). The fiberless cement slabs (30 cm × 30 cm × 0.45 cm) with different coatings were adhered to the central upper surface of 50 cm × 50 cm × 20 cm polyurethane boards (thermal conductivity = 0.02 W/(m K)) using thermal adhesive to create an insulated bottom boundary (Figure 1f). The sides and top of the polyurethane boards were covered with aluminum foil to reflect incident radiation. Subsequently, two thermocouples were secured at one-third intervals along the diagonal of the coating's surface to monitor the surface temperature. Note that the thermocouples were covered by respective coatings to ensure the same radiative conditions as the target coatings. The temperature of coatings was recorded every 1 min using a datalogger (HIOKI, LR8450), and the average value of the two thermocouples was used for each coating. Notably, for coating F, the thermocouples on the surface were covered by aluminum foil rather than the coating until 29 June 2023.

Meteorological parameters, including ambient air temperature (t_{air}, °C), relative humidity (RH, %), total incident solar radiation (I_{sr}, W/m²) and wind velocity (V, m/s), were monitored by a nearby PC-2-T2 meteorological station (Figure 1g) at 1 min interval.

Simulation of building loads

By simulating the application of the seven coatings to the outer surface of roofs in five target cities, the study examined the effects of these coatings on building cooling and heating loads. As material aging is a complex process, this study only considered the efficacy of different coatings at the initial state. That is, for each coating, the input shortwave reflectivity and longwave emissivity are the average values of duplicate samples in their initial state. But the long-term performance can be approximated by changing the coating's radiative properties in the simulation, similar to using another coating with lower shortwave reflectivity and longwave emissivity. Based on the simulation results, the building model exhibited cyclic variations in the thermal behavior from the second year. Therefore, data from the second year were used for analysis. The performance of different coatings applied in the five target cities was compared. The simulation process was as follows.

Simulation tool

WUFI-Plus is the most comprehensive simulation tool in the WUFI® software family. In addition to simulating the hygrothermal conditions within the building envelope and indoor environment, it evaluates parameters related to thermal comfort and energy consumption. Experimental data from studies worldwide have validated its reliability and effectiveness [48–52]. In this study, WUFI-Plus was chosen for simulation. Since only the thermal process was considered, the inherent moisture-related function in the software was deactivated.

Target cities

Simulations were conducted on office buildings in typical Chinese cities with different climatic characteristics to reveal the applicability of the coatings in various regions of China. According to GB 50176–2016 [53], China's thermal design zones are divided into the severe cold zone (SCZ), cold zone (CZ), hot summer and cold winter zone (HSCWZ), hot summer and warm winter zone (HSWWZ) and mild zone (MZ). These thermal design zones are primarily defined based on the average temperatures of the coldest and hottest months, and supplemented by the number of days with a daily average temperature below 5°C or above 25°C. In this study, considering the thermal design zones and the climatic characteristics of each city, Harbin, Beijing, Chongqing, Guangzhou and Kunming were selected as target cities for simulation. The hourly meteorological data, including t_{air}, I_{sr}, V, RH and cloud cover, for the entire typical meteorological year of the five target cities were referenced from the standard JGJ/T 346–2014 [54] and shown in Figures S6–S10.

Model construction

Based on previous research [55], our building load simulation was conducted using WUFI-Plus to construct a

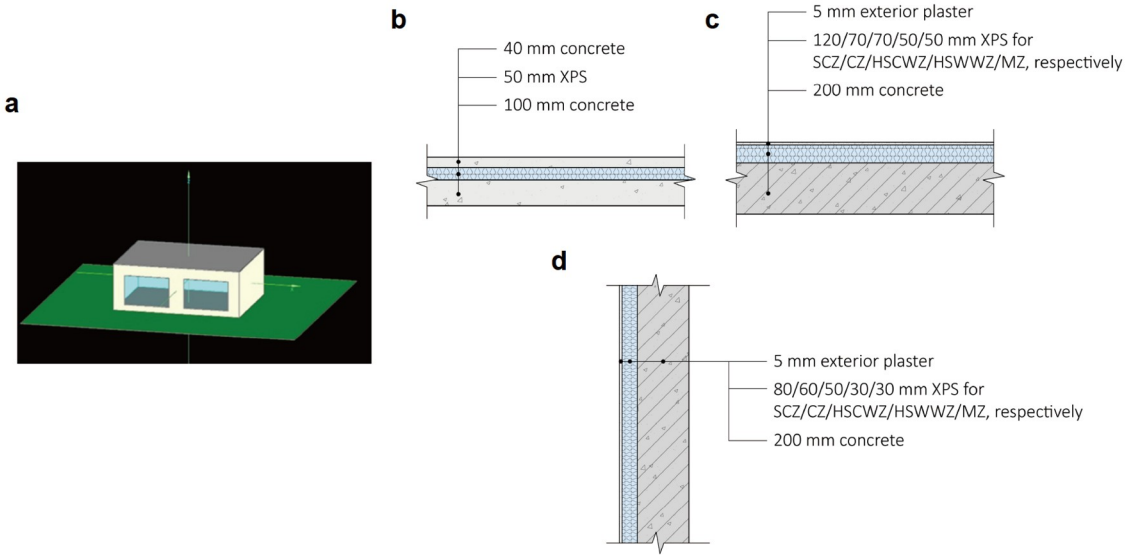


Figure 2 Simulation model and component structures. (a) Simulation model; (b) floor; (c) roof; (d) wall.

building energy simulation test (BESTEST) model from the IEA Annex [56] with inner dimensions of 8 m × 6 m × 2.7 m. The model and its component structures are illustrated in Figure 2. The bulk densities of concrete, extruded polystyrene (XPS) and exterior plaster were 2300, 40, and 1310 kg/m^3, respectively; their thermal conductivities were 1.60, 0.03 and 0.87 W/(m K), respectively; their heat capacities were 850, 1500 and 850 J/(kg K), respectively. The thickness of the XPS insulation layer in the model was determined according to the requirements of GB 50189–2015 [57], with the specific values shown in Figure 2.

Given that this study focused on office buildings, the operation parameters were set solely during office hours (8:00–18:00). During this period, there were five people in the office building. An indoor temperature below 20°C started heating while above 26°C initiated cooling. The air change rate was 1 air change per hour (ACH), and the air infiltration rate was 0.1 ACH. The heat transfer resistance of the inner surface was 0.11 m^2 K/W, and the exterior convective heat transfer coefficient was calculated using Eq. (2).

$$h = 4.5 + aV,\ a = \begin{cases} 1.6 \text{ when windward,} \\ 0.33 \text{ when leeward,} \end{cases} \tag{2}$$

where h is the convective heat transfer coefficient for the exterior surface, W/(m^2 K); a is the correlation coefficient; V is the wind velocity, m/s.

RESULTS AND DISCUSSION

In this section, the surface appearance and radiative properties of the seven coatings were analyzed in detail, both initially and after the temperature cyclic, UV-aging and natural aging tests. Subsequently, the long-term cooling performance of the coatings in field measurements was introduced. Finally, the simulation results for the office building with different coatings on the roof were analyzed and discussed.

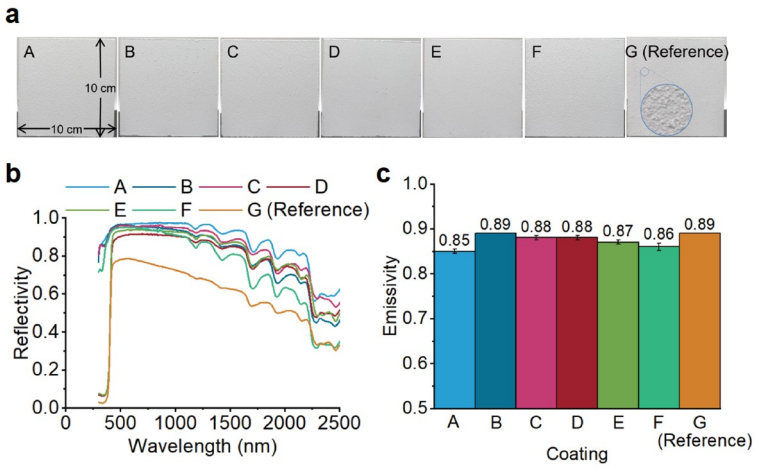


Figure 3 Initial surface appearance and radiative properties of the seven coatings. (a) Surface appearance; (b) spectral reflectivity of the coatings; (c) longwave emissivity of the coatings.

Changes of surface appearance and radiative properties

The surface appearance and radiative properties of the initial coatings are shown in Figure 3. All samples had smooth, flat and purely white surfaces, except for coating G (Reference), which had a powdery texture (Figure 3a and Figure S1). Coatings A, B and C exhibited higher spectral reflectivity in the visible light band compared with other coatings (Figure 3b). Their shortwave reflectivity was 0.95, 0.91 and 0.93, respectively, indicating excellent sunlight reflection ability. The shortwave reflectivity of coatings D, E and F was moderate, at 0.85, 0.88 and 0.90, respectively. Of all coatings, coating G (Reference) had the lowest shortwave reflectivity, merely 0.70. The longwave emissivity of the seven coatings was similar (Figure 3c). Coatings B and G (Reference) had the highest longwave emissivity of 0.89, which was only 0.04 higher than the lowest value (coating A). Based on these measured radiative properties, coatings A–F met the definition of solar radiation control coatings specified in the ASTM C1483/C1483M standard (shortwave reflectivity > 0.80, longwave emissivity > 0.80) [58].

Figure 4 shows the surface changes and radiative properties of the coatings after temperature cyclic test. After 40 cycles, the surfaces of all coatings remained almost unchanged, except for small cracks on coating A and additional powder on coating G (Reference) (Figure 4a). The cracks on coating A may have been caused by mismatched physical properties, such as rigidity and strength, between the fiberless cement slab and the coating, thus leading to exceeded tensile stress between them during the high- and low-temperature cycles. Alternatively, this mismatch may occur after heat expansion and cold contraction under self-stress due to excessive coating thickness. The surface change of coating G (Reference) cannot be fully explained at this moment, but it may lie in some temperature-sensitive components in the coating. The shortwave reflectivity of all coatings fluctuated marginally during the temperature cyclic test but generally remained steady (Figure 4b). Such minor and irregular fluctuation could be attributed to experimental errors. Similarly, although the longwave emissivity of all coatings showed relatively large fluctuations, the decreasing trend remained limited. The variation of the coating's radiative properties was similar to the results obtained by Lei *et al*. [41] (Table S3). Thus, we conclude that the temperature cycles could negatively affect the appearance

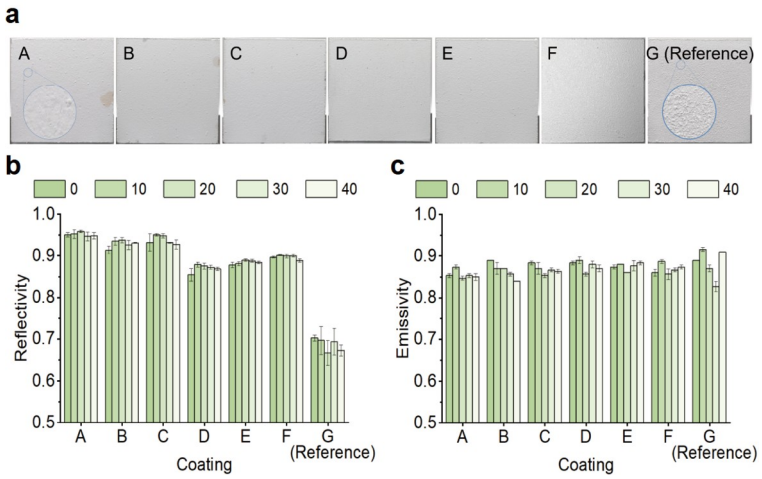


Figure 4 Changes in the surface appearance and radiative properties of the coatings during temperature cyclic test. (a) Surface appearance of the coatings after 40 cycles; (b) shortwave reflectivity of the coatings; (c) longwave emissivity of the coatings.

of coatings A and G (Reference), but only marginally affected the shortwave reflectivity and longwave emissivity of all target coatings.

The surface appearance and radiative properties of the coatings after the UV-aging test are shown in Figure 5. It is clear that only the surface appearance of coating F remained unchanged after 100 h of UV radiation, while all other candidates showed changes to different extents. Specifically, coatings A and C developed some cracks, as the UV exposure may have ruptured chemical bonds within the coating. The cracks on coating C were relatively large, and the coating easily fell off after water spraying. Bubbles appeared on the surface of coating B, probably owing to the inadequate adhesion between the coating and substrate. This was evidenced by the cross-cut test results, where coating B had an initial rate of 4 and even dropped to 5 after UV-aging for 100 h (Figures S4, S5 and Table S1). Nevertheless, it was found that the presence of bubbles on the surface of coating B and cracks on coatings A and C had a relatively minor effect on the shortwave reflectivity. The surfaces of coatings D, E and G (Reference) showed varying degrees of yellowing, which may result from the decomposition of certain chemical substances within the coating under UV radiation to produce chromogenic groups. Unlike the occurrence of cracks or bubbles, this color change led to a noticeable decrease in the shortwave reflectivity of coatings D, E and G (Reference) by 0.08, 0.08 and 0.12, respectively, compared with their initial states. The decrease in the shortwave reflectivity of the coating will inevitably lead to an increase in the solar radiation absorption, thereby increasing the temperature of the coating surface [41].

As the UV-aging time increased to 400 h, the surface appearance and shortwave reflectivity of coating F remained unchanged. Interestingly, the yellowing of coatings D, E and G (Reference) gradually became lighter, and the shortwave reflectivity increased. This may be because continuous UV exposure led to the gradual decomposition of the yellowing groups, but further verification is needed in the future. The surface bubbling and cracking on coatings B and C became more severe. Nonetheless, they did not affect their shortwave reflectivity still. When the UV-aging time increased to 600 h, the surface appearance and shortwave reflectivity of all coatings remained relatively unchanged when compared with those at 400 h. For the longwave emissivity, multiple tests showed visible fluctuations and errors, but the overall trend remained

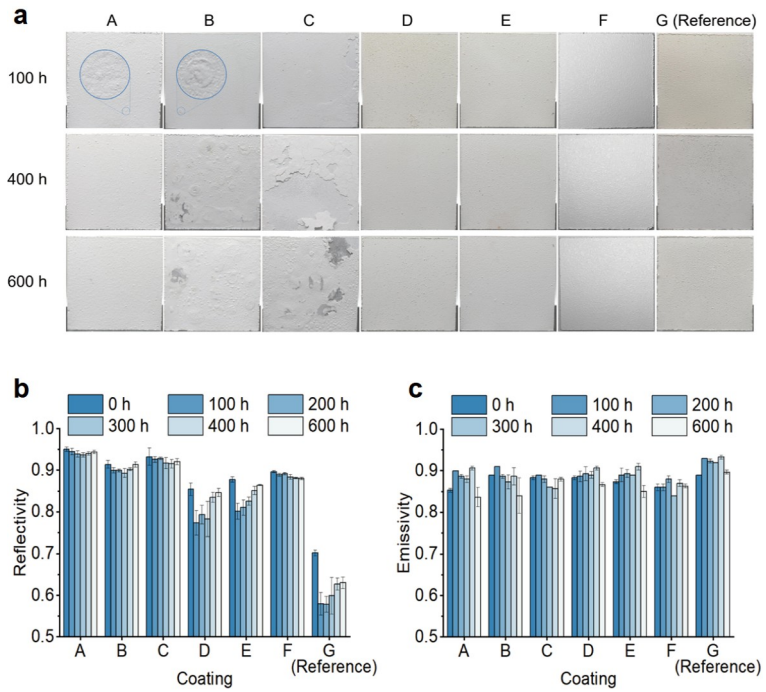


Figure 5 Changes in the surface appearance and radiative properties of the coatings during UV-aging test. (a) Surface appearance of the coating after testing for 100, 400 and 600 h; (b) shortwave reflectivity of the coatings; (c) longwave emissivity of the coatings.

unchanged. Additionally, the surface of coating C was severely damaged, and the degree and location of damage were different for each sample, increasing the measurement errors. Thus, the variations in longwave emissivity were most likely attributable to the changes in appearance and the contact with instrumental sensors. This result was inconsistent with the findings of Xia *et al*. [59], as their radiative cooling coating exhibited a 4.23% reduction in longwave emissivity after 10 cycles of UV-aging. Our results are consistent with other studies, wherein the radiative properties of coatings fluctuated slightly but remained almost unchanged after UV-aging test. However, regarding the surface appearance, other scholars claimed that it remained unaffected by UV-aging (Table S4). In short, during the UV-aging test, the surface appearance of coatings A, B and C was damaged, and the surface color of coatings D, E and G (Reference) turned yellow. Only coating F showed a high resistance to UV-aging.

In contrast to the artificial conditions, the effects of real outdoor environment on the aging of coatings are more complex, with temperature fluctuations, solar radiation, precipitation and dust pollution simultaneously involved [40]. The surface appearance of the coatings on 8 July (two weeks' natural aging) and 19 August (eight weeks) are presented in Figure 6a. On 8 July, the surface appearance of all coatings remained unchanged, except for some cracks on coating C. However, owing to rain and wind, all coatings accumulated dust on their surfaces, which may slightly reduce the shortwave reflectivity and weaken the cooling performance of the coatings [60]. By 19 August, some small cracks appeared on coating A and bubbles appeared on coating B. What is more, coating C exhibited severe cracking and even peeling. This was similar to the results of UV-aging for 100 h (Figure 5a). In addition, the accumulation of dust on all coating surfaces aggravated. To avoid this problem, some researchers suggested enhancing the hydrophobicity of the coatings

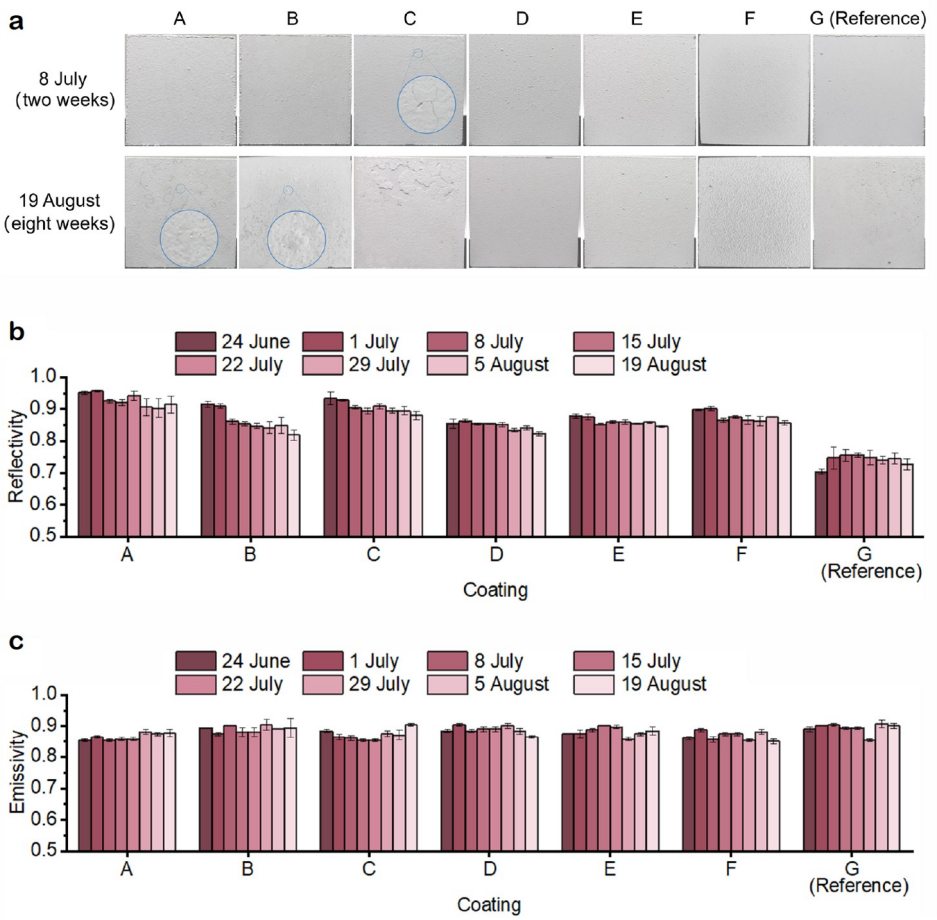


Figure 6 Changes in the surface appearance and radiative properties of the coatings during natural aging test. (a) Surface appearance of the coating on 8 July and 19 August; (b) shortwave reflectivity of the coatings; (c) longwave emissivity of the coatings.

[39].

With increased exposure time, the overall shortwave reflectivity of coatings A–F decreased (Figure 6b), which was inseparable from the influence of solar radiation, precipitation and dust [60,61]. For the results on 19 August, the shortwave reflectivity of coatings A–F decreased from 0.95 to 0.91, 0.91 to 0.82, 0.93 to 0.88, 0.85 to 0.82, 0.88 to 0.84, and 0.90 to 0.86, respectively. Among them, coatings B and C exhibited the highest decrease, with reductions of 0.09 and 0.05, respectively. This implies that their radiative cooling performance should be decreased, as demonstrated in the following section. Coating D showed the smallest decrease, with a reduction of only 0.03. The most notable trend was that the shortwave reflectivity of coating G (Reference) increased first, remained stable for a period, and then decreased. We cannot easily explain this phenomenon, but the radiative properties of coating G (Reference) exhibited the most significant scatters, the same as the situations in the temperature cyclic and UV aging tests. Thus, we speculate on its inherent instability and inhomogeneity. On the contrary, although natural weather negatively affected the surface appearance and the shortwave reflectivity of the coatings, their longwave emissivity fluctuated marginally around the average value (Figure 6c), which is consistent with the conclusions of most reported studies (Table S5). Since shortwave reflectivity and longwave emissivity determine the radiative heat absorption and dissipation of a

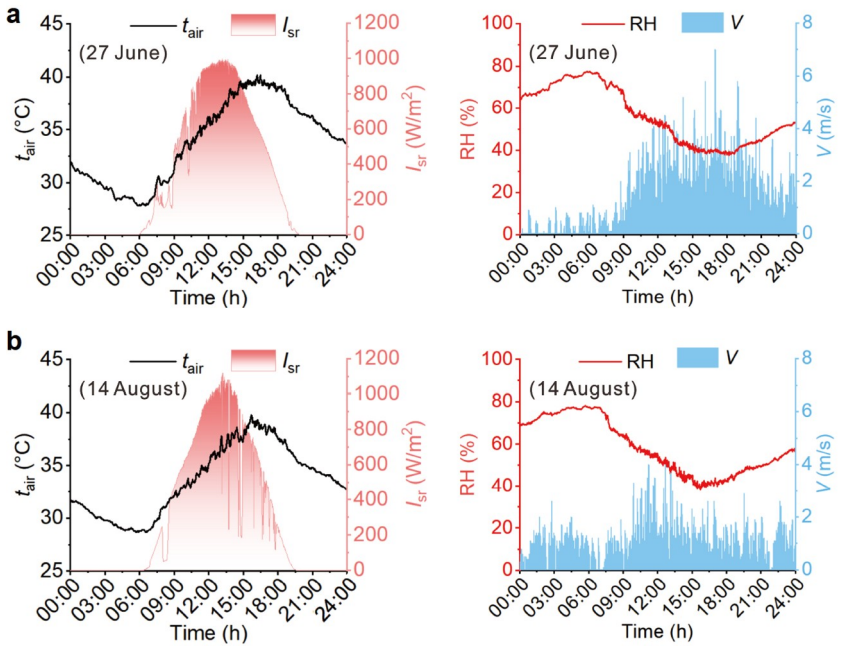


Figure 7 Meteorological parameters on 27 June and 14 August. (a) Weather conditions on 27 June; (b) weather conditions on 14 August.

coating respectively, the variation in the cooling performance during natural aging (in the following section) should be mainly due to the reduction in shortwave reflectivity, independent of the constant longwave emissivity.

Long-term cooling performance

To study the effects of natural aging on the long-term cooling performance of the coatings, the test results on 27 June (the third day of the natural aging test) and 14 August (the 50th day), displaying similar weather conditions, were selected for comparison. Notably, to adhere to normal human activity schedules, we defined the period of 08:00–18:00 as working hours, and 00:00–08:00 and 18:00–24:00 as resting hours in the following sections.

The meteorological parameters for the selected two days are shown in Figure 7. The daily average ambient air temperatures on 27 June and 14 August were 33.9 and 33.6°C, respectively, with a difference of only 0.3°C. The average solar radiation for working hours on 27 June and 14 August was 689 and 682 W/m^2, respectively. Moreover, both days had high noon solar radiation of approximately 1000 W/m^2. The differences in daily average RH and wind velocity were also small, with variations of 2.1% and 0.3 m/s, respectively. In summary, the major meteorological parameters on these two days were highly similar, and it is reasonable to compare the experimental results from the two days.

The measured coatings' and ambient air temperatures on 27 June and 14 August are shown in Figure 8a. The cooling temperatures of different coatings are further illustrated by Figure 8b, where the vertical axis labeled "t_{cool}" (cooling temperature, °C) represents the difference between the coating's surface temperature and the ambient air temperature. As the sun rose at approximately 7:00, the temperatures of the coatings

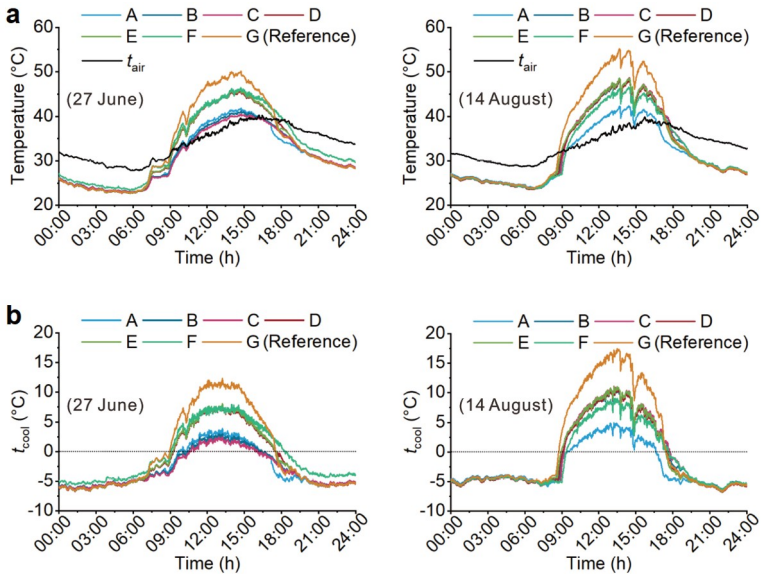


Figure 8 Real-time temperatures and cooling temperatures on 27 June and 14 August. (a) The coatings and ambient air temperatures on 27 June (left) and 14 August (right); (b) cooling temperatures of the coatings on 27 June (left) and 14 August (right).

Table 1 Average measurements in different periods on 27 June and 14 August

Time	Date	Meteorological parameter				Cooling temperature (t_{cool}) (°C)						
		t_{air} (°C)	I_{sr} (W/m^2)	RH (%)	V (m/s)	A	B	C	D	E	F	G (Reference)
00:00–24:00	27 June	33.9	305	56.3	0.9	−2.9	−2.8	−3.0	−1.5	−1.4	−0.4	−0.2
	14 August	33.6	298	58.4	0.7	−2.4	−0.6	−0.5	−0.9	−0.7	−1.2	1.2
8:00–18:00	27 June	36.2	689	50.0	1.4	0.6	0.3	−0.1	3.6	3.8	4.5	6.7
	14 August	35.9	682	50.7	0.8	1.1	5.1	5.4	5.0	5.4	3.8	9.7
00:00–8:00 and 18:00–24:00	27 June	32.3	31	60.9	0.5	−5.3	−5.0	−5.1	−5.2	−5.1	−3.9	−5.1
	14 August	32.0	23	64.0	0.6	−4.9	−4.7	−4.7	−5.1	−5.0	−4.8	−4.8

began to rise and reached their highest points at approximately 14:00, gradually declining to their lowest points after 19:00. Unlike many other reported results, none of our target coatings provided subambient cooling for a full-day. This is because of the intensive solar radiation and high air humidity on both selected days. It should be noted that coating F consistently had a higher temperature at night on 27 June than the other coatings. This should be attributed to the fact that the thermocouples on its surface were covered by aluminum foil, which has a much lower longwave emissivity (0.08). So the cooling performance of coating F was analyzed separately later.

The daily average cooling temperatures on 27 June and 14 August are shown in Table 1. It can be seen that the daily average cooling temperatures of coatings A–G on 27 June were negative, thereby providing overall cooling throughout the day. Coatings A, B and C exhibited better cooling performance compared with other coatings, with cooling temperatures of −2.9, −2.8 and −3.0°C, corresponding to their top three rankings in shortwave reflectivity (Figure 3b). Coatings D and E ranked in the middle, whereas coating G (Reference) exhibited the lowest daily average cooling temperature of −0.2°C. By 14 August, the cooling performance of all coatings decreased owing to natural aging. The results were similar to those of Dong *et al*. [62], Lei *et al*. [41], etc., wherein the cooling ability of the coating declined after a period of natural exposure (Table S6), but

just the opposite of the results of Cai *et al*. [23]. This may be that Cai *et al*. used the minimum value of the cooling temperature, and their results were instantaneous, unable to fully represent the cooling performance over a period of time. Coatings A, D and E comprised the top three in terms of daily average cooling temperatures, at −2.4, −0.9 and −0.7°C, respectively. Coatings B and C ranked fifth and fourth, respectively. Coating G (Reference) unsurprisingly exhibited the poorest daily average cooling temperature of 1.2°C. The excellent long-term cooling performance of coating A can be explained by its consistently high shortwave reflectivity compared with the other coatings. Although coatings B and C initially had high shortwave reflectivity and longwave emissivity, their shortwave reflectivity decreased the fastest during the natural aging test (Figure 6b), and the surface suffered irreversible damage (Figure 6a). This resulted in an obvious reduction in its cooling performance. In contrast, the shortwave reflectivity of coatings D and E decreased at a slower rate, and the surface appearance remained acceptable, allowing them to outperform coatings B and C in cooling performance on 14 August. Coating G (Reference) consistently exhibited the lowest shortwave reflectivity all the time, leading to poor cooling performance. It is worth emphasizing that the cooling ability of the coatings was not completely ordered by the shortwave reflectivity, because it was also affected by the longwave emissivity [63]. If the coatings have the same shortwave reflectivity, those with higher longwave emissivity would exhibit better cooling performance.

The variation trend in the cooling temperature during working hours (Table 1) was mostly consistent with that of the full-day test results. A small difference existed in that the daily average cooling performance of coating B was worse than that of coating E on 14 August, but the average cooling performance of coating B was better during working hours, with a difference of only 0.3°C. This may result from the unstable surface appearance of coating B (Figure 6a). The average cooling temperatures during working hours of all coatings were notably positive on the selected two days, except for coating C on 27 June. The average cooling performance during working hours on 14 August was even worse on 27 June owing to natural aging, which increased the absorption of solar radiation and therefore rendered insufficient cooling.

Contrary to the situation during working hours, all coatings provided subambient cooling of approximately 5°C during resting hours (Table 1). Because of limited or absent solar radiation during resting hours, the longwave emissivity of the coatings had a more significant effect on the cooling performance than the shortwave reflectivity. The initial longwave emissivity of all coatings was close (Figure 3c), so the differences in cooling performance during resting hours among the coatings were negligible on 27 June, as the maximum cooling temperature (coating A) was only 0.3°C lower than the minimum one (coating B). The cooling performance of all coatings during resting hours on 14 August was worse than that on 27 June. However, natural aging tests showed minimal changes in the longwave emissivity with extended outdoor exposure time. Consequently, the reduction of cooling performance in resting hours was very small.

The average cooling temperature of coating F on 14 August was consistently lower than that on 27 June regardless of the period. This was because the thermocouples for surface temperature determination were covered by aluminum foil rather than the coating on 27 June. The aluminum foil used was low in both shortwave reflectivity (0.64) and longwave emissivity (0.08), thereby absorbing more solar radiation and emitting less thermal radiation. Consequently, the cooling temperature of coating F on 27 June was not comparable to those of the other coatings. However, on 14 August, after the thermocouples being covered by the coating, the roof model F was no longer significantly different from the others. For the full-day and working hour periods, the cooling performance of coating F was second only to that of coating A, thanks to

the slow reduction in its shortwave reflectivity and the stable surface appearance during the natural aging process (Figure 6). Given that the initial longwave emissivity of coating F was the second lowest (Figure 3c) and remained relatively low throughout the natural aging test (Figure 6c), the cooling performance of coating F at night ranked only fifth.

In short, during the early stages of the field measurements, coatings A, B and C exhibited superior cooling performance owing to their high shortwave reflectivity (coating F was not included in the ranking). However, in the later stages, the shortwave reflectivity of coatings B and C experienced a rapid decline, along with the bubbling and peeling. Contrarily, the shortwave reflectivity and surface appearance of coatings D and F were relatively stable. Thus, the cooling performance of coatings A, D and F became superior. Coating G (Reference) consistently exhibited the poorest cooling performance because of its low shortwave reflectivity and longwave emissivity.

As for future improvement, both laboratory tests and field measurements showed that the radiative properties of coating A were commendable, especially its long-term performance. However, coating A was low in longwave emissivity and readily developed fine cracks. The initial shortwave reflectivity and longwave emissivity of coatings B and C were relatively high, but their radiative properties declined rapidly and the surface appearance was unstable during the aging process, resulting in a marked decline in cooling performance with time. Coatings D and E maintained stable surface appearance but were prone to discoloration when exposed to UV radiation, further reducing their non-advantageous shortwave reflectivity and cooling performance. Coating F exhibited a stable surface appearance and demonstrated strong resistance to all environmental factors. In future research, if the radiative properties of coating F can be further improved, it will represent an excellent cooling coating. As for coating G (Reference), its radiative properties, resistance to UV radiation and natural aging require considerable improvement.

Simulation results

The cooling and heating loads of the office buildings with different coatings on the roof in the five target cities are shown in Figure 9. In general, regarding the cooling load, Guangzhou ranked first (the cooling load of the office buildings with coatings A–G on the roof were 28.2, 28.8, 28.5, 30.1, 29.7, 29.3 and 33.5 kWh/m^2, respectively) and Harbin was the last (the cooling load using coatings A–G were 0.8, 0.8, 0.8, 1.0, 0.9, 0.9 and 1.3 kWh/m^2, respectively). Contrarily, Harbin had the highest heating load (with the lowest value up to 222.9 kWh/m^2 obtained by using coating G (Reference)), while Guangzhou had the lowest heating load (the highest value was only 24.8 kWh/m^2, which was also obtained when coating G (Reference) was used). This could be easily explained by their dramatic differences in climate. Owing to Kunming's mild climate, no cooling load was observed regardless of the type of coating used. The cooling loads with different coatings in the target cities (excluding Kunming) exhibited similar trends (Figure 9a). The buildings with coatings A, B and C exhibited the lowest cooling load while buildings with coating G (Reference) had the highest cooling load in all cities. This is because coatings A, B and C have higher shortwave reflectivity than the other coatings but with limited differences in longwave emissivity (Figure 3), thereby demonstrating effectiveness in reducing solar radiation absorption and hence the cooling load. For the heating load, the trend was opposite to that of the cooling load and this could be similarly explained. It should be further emphasized that the load differences in using various coatings in this study seem not significant, reaching 5.3 kWh/m^2 for

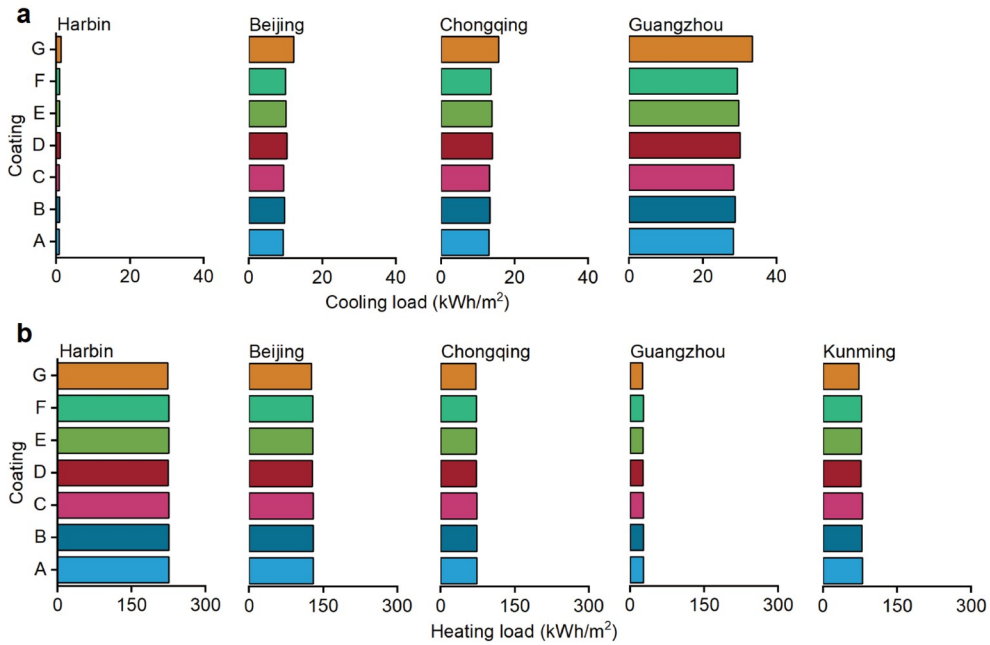


Figure 9 Cooling and heating loads using different coatings on the roof of office buildings in five target cities. (a) Cooling load (no cooling load in Kunming); (b) heating load.

the cooling load in Guangzhou at maximum. This is because all building envelopes were well insulated during the modeling. If the insulation layer is thinner or removed, the contribution of the coating will increase [55]. In other words, to maintain the same cooling load, the use of radiative cooling coatings can reduce the need for insulation layers.

It is worth mentioning that in practical applications coatings commonly face aging, resulting in changes in their radiative properties and influencing the cooling and heating loads of buildings. The initial longwave emissivity of all target coatings was similar, and the longwave emissivity remained relatively constant through outdoor exposure. Therefore, when studying the effects of aging on building load, it is reasonable to only consider the changes in shortwave reflectivity. During the natural aging test, the shortwave reflectivity of all coatings continued to decline. Therefore, it is challenging to provide a definitive description of the building load after the aging has occurred. But as mentioned before, an approximation approach is to change the coating's radiative properties after a certain period of time in the simulation, such as replacing coating A by coating D first and then G to represent different aging periods of coating A. Last but not least, the use of cooling coatings can reduce the cooling load of buildings and improve energy efficiency in summer. However, using such coatings during cold seasons inevitably increases the heating load. It is therefore not straightforward whether the annual energy consumption is increased or decreased. For instance, using coating A could reduce the cooling load by 0.5 kWh/m^2 compared with using coating G (Reference) in Harbin, but it will increase the heating load by 2.9 kWh/m^2. However, in Guangzhou, the reduction in cooling load (5.3 kWh/m^2) using coating A was higher than the increase in heating load (2.4 kWh/m^2) compared with using coating G (Reference). To resolve this problem, appropriate coating with balanced radiative properties should be selected based on the building's thermal characteristics, operation requirements and local climate [55]. A more promising solution is to employ smart coating control systems, which could automatically

adjust the radiative properties of the coating based on climatic conditions to minimize annual energy consumption [64].

CONCLUSIONS

In this study, we conducted laboratory and outdoor measurements to determine the weather resistance of seven different coatings (A–G) through temperature cyclic, UV-aging and natural aging tests. The effect of coating aging on cooling performance was also studied through long-term field measurements. WUFI-Plus was finally used to simulate building load when different coatings were applied to the roofs of office buildings in various climate zones in China. The following conclusions were drawn.

(1) The temperature cycles had different impacts on varied coatings. It had relatively no adverse effects on the surface appearance of coatings B–F, but produced small cracks on coating A and powder on coating G (Reference). Temperature cycles had only a marginal effect on the radiative properties of all target coatings.

(2) Most coatings were sensitive to UV. In the UV-aging test, only the radiative properties and surface appearance of coating F remained virtually unchanged. The surfaces of coatings D, E and G (Reference) turned yellow, and their shortwave reflectivity decreased. Coatings A, B and C exhibited varying degrees of surface cracking or peeling, which did not affect their radiative properties though.

(3) Natural aging led to deterioration in most coatings' shortwave reflectivity. After two months' outdoor exposure, fine cracks appeared on coating A and bubbles appeared on coating B. Coating C experienced considerable peeling. The shortwave reflectivity of coatings A–F decreased, with coatings B and C exhibiting the fastest declines. Only coating G (Reference) was nearly unaffected. The longwave emissivity of all coatings remained unchanged.

(4) The long-term cooling performance was correlated with the coating's aging sensitivity. Coatings A, B and C initially exhibited the best cooling performance owing to the advantageous initial shortwave reflectivity, with daily average cooling temperatures of −2.9, −2.8 and −3.0°C, respectively (coating F was not included in the ranking). However, aging had a significant effect on coatings B and C, while coatings D and F demonstrated superior anti-aging capability. The cooling performance of coatings A, D and F was the best in the later period. Coating G (Reference) consistently showed the worst performance throughout the experiment due to its low shortwave reflectivity and longwave emissivity.

In summary, this study conducted an in-depth investigation on seven cooling coating candidates and explored their weather resistance, long-term cooling performance and ability to reduce building load. Each coating demonstrated pros and cons, and future research should focus on improving coatings' weathering resistance. The results of this research provide valuable information for further development in radiative cooling technology.

Data availability

The original data are available from corresponding authors upon reasonable request.

Funding

This work was supported by the Fundamental Research Funds for the Central Universities (2023CDJXY-008).

Author contributions

C.F., Y.H. and B.L. designed the research. Y.H., B.L. and Y.L. did the experiments and analyzed the data. J.F. did the simulation. Y.H. wrote the manuscript. C.F. and S.G. revised the manuscript.

Conflict of interest

The authors declare no conflict of interest.

Supplementary information

The supporting information is available online at https://doi.org/10.1360/nso/20230065. The supporting materials are published as submitted, without typesetting or editing. The responsibility for scientific accuracy and content remains entirely with the authors.

References

1 Song Z, Zhang W, Shi Y, *et al.* Optical properties across the solar spectrum and indoor thermal performance of cool white coatings for building energy efficiency. *Energy Buildings* 2013; **63**: 49–58.

2 Zhang Y, Yang Z, Zhang Z, *et al.* Sub-ambient cooling effect and net energy efficiency of a super-amphiphobic self-cleaning passive sub-ambient daytime radiative cooling coating applied to various buildings. *Energy Buildings* 2023; **284**: 112702.

3 Yu S, Zhang Q, Wang Y, *et al.* Photonic-structure colored radiative coolers for daytime subambient cooling. *Nano Lett* 2022; **22**: 4925–4932.

4 Parker DS, Barkaszi Jr. SF. Roof solar reflectance and cooling energy use: Field research results from Florida. *Energy Buildings* 1997; **25**: 105–115.

5 Sharma R, Tiwari S, Tiwari SK. Highly reflective nanostructured titania shell: A sustainable pigment for cool coatings. *ACS Sustain Chem Eng* 2018; **6**: 2004–2010.

6 Synnefa A, Santamouris M, Livada I. A study of the thermal performance of reflective coatings for the urban environment. *Sol Energy* 2006; **80**: 968–981.

7 Zhang Y, Long E, Li Y, *et al.* Solar radiation reflective coating material on building envelopes: Heat transfer analysis and cooling energy saving. *Energy Explor Exploitation* 2017; **35**: 748–766.

8 Guo W, Qiao X, Huang Y, *et al.* Study on energy saving effect of heat-reflective insulation coating on envelopes in the hot summer and cold winter zone. *Energy Buildings* 2012; **50**: 196–203.

9 Triano-Juárez J, Macias-Melo EV, Hernández-Pérez I, *et al.* Thermal behavior of a phase change material in a building roof with and without reflective coating in a warm humid zone. *J Building Eng* 2020; **32**: 101648.

10 Shi NN, Tsai CC, Camino F, *et al.* Keeping cool: Enhanced optical reflection and radiative heat dissipation in Saharan silver ants. *Science* 2015; **349**: 298–301.

11 Raman AP, Anoma MA, Zhu L, *et al.* Passive radiative cooling below ambient air temperature under direct sunlight. *Nature* 2014; **515**: 540–544.

12 Zhao B, Hu M, Ao X, *et al.* Radiative cooling: A review of fundamentals, materials, applications, and prospects. *Appl Energy* 2019; **236**: 489–513.

13 Wijesuriya S, Kishore RA, Bianchi MVA, *et al.* Potential energy savings benefits and limitations of radiative cooling coatings for U.S. residential buildings. *J Cleaner Production* 2022; **379**: 134763.

14 Li W, Li Y, Shah KW. A materials perspective on radiative cooling structures for buildings. *Sol Energy* 2020; **207**: 247–269.

15 Li T, Zhai Y, He S, *et al.* A radiative cooling structural material. *Science* 2019; **364**: 760–763.

16 Ju H, Lei S, Wang F, *et al.* Daytime radiative cooling performance and building energy consumption simulation of

superhydrophobic calcined kaolin/poly(vinylidene fluoride-co-hexafluoropropylene) coatings. *Energy Buildings* 2023; **292**: 113184.

17 Cao J, Xu H, Li X, *et al.* Colored daytime radiative cooling textiles supported by semiconductor quantum dots. *ACS Appl Mater Interfaces* 2023; **15**: 19480–19489.

18 Pakdel E, Wang X. Thermoregulating textiles and fibrous materials for passive radiative cooling functionality. *Mater Des* 2023; **231**: 112006.

19 Xie X, Liu Y, Zhu Y, *et al.* Enhanced IR radiative cooling of silver coated PA textile. *Polymers* 2022; **14**: 147.

20 Yao Z, Xia Q, Ju P, *et al.* Investigation of absorptance and emissivity of thermal control coatings on Mg–Li alloys and OES analysis during PEO process. *Sci Rep* 2016; **6**: 29563.

21 Li H, Lu S, Qin W, *et al. In-situ* grown MgO-ZnO ceramic coating with high thermal emittance on Mg alloy by plasma electrolytic oxidation. *Acta Astronaut* 2017; **136**: 230–235.

22 Cui Z, Guo C, Zhao D. Energy-saving and economic analysis of passive radiative sky cooling for telecommunication base station in China. *Build Simul* 2022; **15**: 1775–1787.

23 Cai Y, Yang Z, Zhang Z, *et al.* Long-term cooling effects and cooling energy conservation of a subambient daytime radiative cooling coating relative to a cool-white coating over distributed telecommunication base stations. *Sol Energy* 2023; **256**: 127–139.

24 Chen J, Lu L. Comprehensive evaluation of thermal and energy performance of radiative roof cooling in buildings. *J Building Eng* 2021; **33**: 101631.

25 Muselli M. Passive cooling for air-conditioning energy savings with new radiative low-cost coatings. *Energy Buildings* 2010; **42**: 945–954.

26 Tang K, Dong K, Li J, *et al.* Temperature-adaptive radiative coating for all-season household thermal regulation. *Science* 2021; **374**: 1504–1509.

27 Jiang T, Fan W, Wang F. Long-lasting self-cleaning daytime radiative cooling paint for building. *Colloids Surfs A-Physicochem Eng Aspects* 2023; **666**: 131296.

28 Liu L, Zhang H, Cai Y, *et al.* Super-amphiphobic coatings with sub-ambient daytime radiative cooling—Part 2: Cooling effect under real conditions. *Sol Energy Mater Sol Cells* 2022; **241**: 111736.

29 Chen J, Lu L, Gong Q, *et al.* Development of a new spectral selectivity-based passive radiative roof cooling model and its application in hot and humid region. *J Cleaner Production* 2021; **307**: 127170.

30 Zhu L, Raman AP, Fan S. Radiative cooling of solar absorbers using a visibly transparent photonic crystal thermal blackbody. *Proc Natl Acad Sci USA* 2015; **112**: 12282–12287.

31 Lee M, Kim G, Jung Y, *et al.* Photonic structures in radiative cooling. *Light Sci Appl* 2023; **12**: 134.

32 Gao W, Lei Z, Wu K, *et al.* Reconfigurable and renewable nano-micro-structured plastics for radiative cooling. *Adv Funct Mater* 2021; **31**: 2100535.

33 Zhai Y, Ma Y, David SN, *et al.* Scalable-manufactured randomized glass-polymer hybrid metamaterial for daytime radiative cooling. *Science* 2017; **355**: 1062–1066.

34 Liu H, Zhu SN. Hierarchical-morphology metafabric for scalable passive daytime radiative cooling. *Chin Sci B-Chin* 2021, **66**: 3787–3790.

35 Chae D, Kim M, Lim H, *et al.* Selectively emissive fluoropolymer film for passive daytime radiative cooling. *Optical Mater* 2022; **128**: 112273.

36 Ishii S, Hernández-Pinilla D, Tanjaya NK, *et al.* Highly reflective multilayer solar reflectors for daytime radiative cooling. *Sol Energy Mater Sol Cells* 2023; **259**: 112463.

37 Fan W, Gao Q, Xiang J, *et al.* Synergistic effect of silica aerogel and titanium dioxide in porous polyurethane composite coating with enhanced passive radiative cooling performance. *Prog Org Coatings* 2023; **183**: 107763.

38 Luo CL, Zheng LX, Jiao JY, *et al.* Enhanced passive radiative cooling coating with Y_2O_3 for thermal management of building. *Optical Mater* 2023; **138**: 113710.

39 Song J, Zhang W, Sun Z, *et al.* Durable radiative cooling against environmental aging. *Nat Commun* 2022; **13**: 4805.

40 Sleiman M, Kirchstetter TW, Berdahl P, *et al.* Soiling of building envelope surfaces and its effect on solar reflectance—Part II: Development of an accelerated aging method for roofing materials. *Sol Energy Mater Sol Cells* 2014; **122**: 271–281.

41 Lei Y, Huang X, Li X, *et al.* Impact of aging, precipitation, and orientation on performance of radiative cooling for building envelope: A field investigation. *Energy Buildings* 2023; **279**: 112716.

42 He Y, Xia Z, Wang R, *et al.* An easily prepared and long-term effective cooling coating that can be cooled to sub-ambient temperature without polyethylene film. *Sol Energy* 2022; **246**: 1–13.

43 Chen M, Pang D, Yan H. Sustainable and self-cleaning bilayer coatings for high-efficiency daytime radiative cooling. *J Mater Chem C* 2022; **10**: 8329–8338.

44 Bijarniya JP, Sarkar J, Tiwari S, *et al.* Development and degradation analysis of novel three-layered sustainable composite coating for daytime radiative cooling. *Sol Energy Mater Sol Cells* 2023; **257**: 112386.

45 Standard tables for reference solar spectral irradiances: Direct normal and hemispherical on 37° tilted surface. ASTM G173–23.

46 Test method for temperature change resistance of architectural coatings. JG/T 25–2017.

47 Paints and varnishes—Artificial weathering and exposure to artificial radiation—Exposure to filtered xenon-arc radiation. GB/T 1865–2009/ISO 11341:2004.

48 Fang J, Zhang H, Ren P, *et al.* Influence of climates and materials on the moisture buffering in office buildings: A comprehensive numerical study in China. *Environ Sci Pollut Res* 2022; **29**: 14158–14175.

49 Hema C, Messan A, Lawane A, *et al.* Impact of the design of walls made of compressed earth blocks on the thermal comfort of housing in hot climate. *Buildings* 2020; **10**: 157.

50 Winkler M, Pazold M, Zegowitz A, *et al.* Use of a radiator for user-centric cooling—Measurement and simulation. *E3S Web Conf* 2020; **172**: 03002.

51 Frasca F, Cornaro C, Siani AM. Performance assessment of a heat and moisture dynamic simulation model in IDA ICE by the comparison with WUFI Plus. *IOP Conf Ser-Mater Sci Eng* 2018; **364**: 012024.

52 Libralato M, De Angelis A, Tornello G, *et al.* Evaluation of multiyear weather data effects on hygrothermal building energy simulations using WUFI plus. *Energies* 2021; **14**: 7157.

53 Code for thermal design of civil building. GB 50176–2016.

54 Standard for weather data of building energy efficiency. JGJ/T 346–2014.

55 Feng C, Lei Y, Fang J, *et al.* Optimized radiative parameters of building roof surfaces for energy efficiency: Case studies in China. *J Building Eng* 2022; **61**: 105289.

56 Judkoff R, Neymark J. International energy agency building energy simulation test (BESTEST) and diagnostic method. 1995, https://digital.library.unt.edu/ark:/67531/metadc793064/m2/1/high_res_d/90674.pdf.

57 Design standard for energy efficiency of public buildings. GB 50189–2015.

58 Specification for exterior solar radiation control coatings on buildings. ASTM C1483/C1483M-17.

59 Xia S, Wang F, Yang S, *et al.* Water-based kaolin/polyacrylate cooling paint for exterior walls. *Colloids Surfs A-Physicochem Eng Aspects* 2023; **677**: 132401.

60 Yue X, Wu H, Zhang T, *et al.* Superhydrophobic waste paper-based aerogel as a thermal insulating cooler for building. *Energy* 2022; **245**: 123287.

61 Standard practice for laboratory soiling and weathering of roofing materials to simulate effects of natural exposure on solar reflectance and thermal emittance. ASTM D7897–18.

62 Dong Y, Zou Y, Li X, *et al.* Introducing masking layer for daytime radiative cooling coating to realize high optical performance, thin thickness, and excellent durability in long-term outdoor application. *Appl Energy* 2023; **344**: 121273.

63 Feng C, Lei Y, Huang X, *et al.* Experimental and theoretical analysis of sub-ambient cooling with longwave radiative coating. *Renew Energy* 2022; **193**: 634–644.

64 Wang J, Xie M, An Y, *et al.* All-season thermal regulation with thermochromic temperature-adaptive radiative cooling coatings. *Sol Energy Mater Sol Cells* 2022; **246**: 111883.